



AENSI Journals

Australian Journal of Basic and Applied Sciences

Journal home page: www.ajbasweb.com

A Localised Cloud Detection and Masking Method Using Spectral Analysis

¹Asmala Ahmad, ¹Burhanuddin Mohd. Aboobaidar, ¹Mohd. Khanapi Abdul Ghani, ¹Sazalinsyah Razali, ²Saari Mohamad Isa, ³Noorazuan Md. Hashim

¹Department of Industrial Computing, Faculty of Information and Communication Technology, Universiti Teknikal Malaysia Melaka, Malaysia.

²Department of Telecommunication Engineering, Faculty of Electrical Engineering, Universiti Teknikal Malaysia Melaka, Malaysia.

³School for Social, Development and Environmental Studies, Universiti Kebangsaan Malaysia, Malaysia.

ARTICLE INFO

Article history:

Received 1 October 2013

Received in revised form 18

December 2013

Accepted 29 December 2013

Available online 1 February 2014

Key words:

Cloud, Masking, MODIS, Spectral, Threshold

ABSTRACT

In satellite remote sensing, cloud blocks surface or near surface information. The aim of this study is to investigate the spectral properties of cloud and to carry out cloud detection and masking over Malaysia based on spectral analysis. A cloud detection and masking method tuned to tropical conditions have been developed based on spectral of MODIS (Moderate Resolution Imaging Spectroradiometer) data. Thresholds were applied to three sets of spectral measurements, i.e. reflective bands, thermal bands and brightness temperature difference of thermal bands. The results show that the method was able to detect clouds over Malaysia effectively.

© 2013 AENSI Publisher All rights reserved.

To Cite This Article: Asmala Ahmad, Burhanuddin Mohd. Aboobaidar, Mohd. Khanapi Abdul Ghani, Sazalinsyah Razali, Saari Mohamad Isa, Noorazuan Md. Hashim., A Localised Cloud Detection and Masking Method Using Spectral Analysis. *Aust. J. Basic & Appl. Sci.*, 7(14):3-10, 2013

INTRODUCTION

Over 60 per cent of the Earth's surface is covered by cloud at any time (Choi and Ho, 2009), where a cloud is a visible mass of condensed water droplets or ice crystals suspended in the atmosphere above the Earth's surface. Cloud is made of either water droplets or ice particles or both with diameters ranging from 10 to several hundreds μm . It scatters electromagnetic energy in UV through mid-infrared wavelengths due to the much larger particle diameter than the wavelengths and therefore causing Mie scattering. This leads to the two most obvious features of clouds seen from space; they are white and bright. Cloud detection from satellites data is based on radioactive properties in visible and thermal infrared spectral range. Cloud appears brighter in the visible wavelengths due to the shorter path of the photon come from the sun and reflected by cloud particles towards the satellite sensor, than in a cloud-free atmosphere, while darker in the thermal wavelengths due to the lower temperature than the surroundings (Jose *et al.* 2003). The primary cloud types are cumulus, stratus and cirrus. Those further classified from the main types include cumulonimbus, nimbostratus, stratocumulus, altocumulus and cirrocumulus; depending on their height and appearance from ground, i.e. cirro- (curl), alto- (mid), strato- (layer), nimbo- (precipitation) and cumulo- (heap).

In remote sensing, thick opaque cloud blocks almost all information from the surface or near surface, while thin cloud has some physical characteristics similar to other atmospheric constituents. Misinterpretation of cloud may result in inaccuracy of various remote sensing applications, ranging from land cover classification to retrieval of atmospheric constituents (Hashim *et al.*, 2004; Ahmad and Quegan, 2012; Ahmad and Sufahani, 2012; Ahmad and Quegan, 2013). Several cloud detection and masking studies have been reported in the literature. However, most of these algorithms were designed for the global scale (Rossow and Gardner, 1993; Ackerman *et al.*, 2002) and little effort has been devoted to optimizing regional methods. Some regional cloud masking algorithms have been designed for high, low and mid latitude regions, and these customized cloud masking algorithms tend to work best for these regions (Saunders, 1986; Logar *et al.*, 1998). Little serious effort has been applied to the equatorial regions, especially South-east Asia (Bendix *et al.*, 2004). This study considers this issue for the particular case of Malaysia. It uses MODIS Terra data to examine the spectral behaviour of cloud and uses effective MODIS bands for cloud detection in this region.

Cloud Detection from Satellites:

Cloud detection from satellites data is based on radiative properties in visible and thermal infrared spectral

Corresponding Author: Asmala Ahmad, Department of Industrial Computing, Faculty of Information and Communication Technology, Universiti Teknikal Malaysia Melaka, Malaysia.
Email: asmala@utem.edu.my

range. Cloud appears very brighter in the visible wavelengths due to the shorter path of the photon come from the sun and reflected by cloud particles towards the satellite sensor, than in a cloud-free atmosphere, while darker in the thermal wavelengths due to the lower temperature than the surroundings (Jose *et al.*, 2003). In visible wavelengths, the larger the water content and the thicker the cloud, the higher the reflectance measured from the satellite sensor, therefore it appears brighter (Li *et al.* 2003). The convective clouds look brighter than the stratiform clouds because they contain more water droplets and are thicker. Among the convective clouds, cumulonimbus is brighter than cumulus. Hence, in most cases, cloud formed in the lower levels is brighter than the higher levels. In near infrared wavelengths, a cloud with high cloud top height looks bright and a cloud with low cloud top height look dark. Among the stratiform clouds, high level clouds are the brightest, followed by middle level clouds and low level clouds. In terms of forms, a stratiform cloud often appears with fairly large extent of cloud area, while the convective cloud exists as a rather small cloud cluster. In terms of texture, a stratiform cloud has a smooth and even cloud surface, while a convective cloud has an uneven and ragged cloud surface.

Due to the higher reflectance and lower temperature values than land, cloud can be identified by selecting threshold values that denote the lowest cloud reflectance and the highest cloud temperature in an image (Bendix *et al.* 2004). The exceptions to this rule in the visible wavelengths are snow, ice, and white sand, which can have reflectance values that are greater than or equal to the cloud reflectance values (Di Vittorio and Emery 2002). Such exceptions can be ignored, as most of the study areas are highly vegetated land areas. Clouds have higher optical thicknesses in the visible spectral range compared to all other atmospheric constituents such as haze and fog; therefore often block the surface from the solar radiation. Cloud, can consist of water or ice droplets, often have different spectral properties at different wavelengths so requires different spectral bands with appropriate thresholds. The spectral properties of cloud over land differ significantly from ocean. Hence, using different thresholds for such conditions tends to give better results than using the same thresholds. Most of cloud detection scheme employs cloud detection algorithm involving a number of tests which are based on differences between the spectral properties of cloud and non-cloud features. The tests are applied to each pixel within a satellite field-of-view, where the pixels that are flagged as cloud in some of the tests are judged as cloudy; in other words only those identified as cloud-free pixels in every test are judged to be cloud-free. In day time, both visible and thermal bands of the satellite data can be used, so detection of cloud is more informative than night time. Generally high and thick clouds are easier to detect than others. The accuracy of cloud detection depends very much on the properties of the underlying surface. Higher accuracy can be gained for remote sensing data covering surfaces having fairly constant temperature and emissivity (Saunders 1986). This is due to the little variation of the spectral properties for these surfaces; this provides a quite constant difference between them and those of the cloud.

MATERIALS AND METHODS

This study makes use of the MOD021KM product from MODIS Terra satellite. A major advantage of MODIS is its wide range of spectral bands, with 36 spectral bands covering the visible, near infrared and thermal infrared wavelengths. In addition, MODIS, with its swath width of 2330 km, is capable of recording every point on the Earth at least once every two days and has an equatorial crossing time of 10:30 a.m. local time. Thus it can cover the whole study area (Peninsular Malaysia) in a single day pass with a high frequency of revisit. MOD021KM contains data in the form of: (1) radiance ($\text{Wm}^{-2}\mu\text{m}^{-1}\text{sr}^{-1}$) for reflective bands; (2) radiances ($\text{Wm}^{-2}\mu\text{m}^{-1}\text{sr}^{-1}$) for emissive bands; and (3) reflectance (dimensionless) for reflective bands. Peninsular Malaysia is located within $6^{\circ}47'$ N, $88^{\circ}25'$ E (upper left), and $1^{\circ}21'$ N, $106^{\circ}20'$ E (lower right). The haze-free data used in this study is within the South-east Monsoon season dated 30th January 2004. Visual analysis was carried out on individual bands and on band combinations (i.e. three bands displayed simultaneously in the red, green and blue channels) prior to further processing. Cloud appears brighter than the surrounding background in the visible spectral region, while it appears darker in the thermal spectral region because of its low cloud-top temperature. This guided the development of cloud detection methods based on spectral analysis.

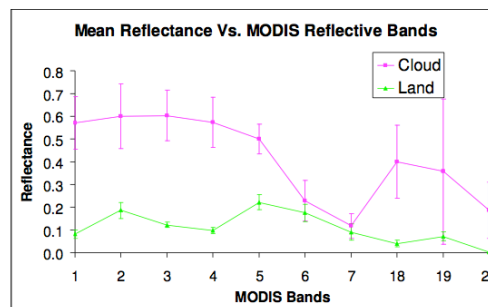
RESULTS AND DISCUSSION

Cloud Detection Using Single Reflective Bands:

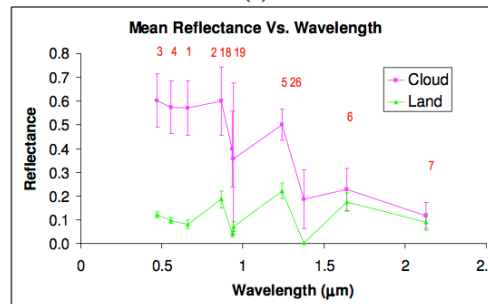
Reflectance curves for cloud, land and ocean for all 20 MODIS reflective bands are plotted in Fig. 1, and the mean reflectance for cloud, ocean and land against the MODIS bands and wavelengths, are shown in Table 1. Bands with negative values, due to saturation, have been omitted.

Table 1: Cloud and land mean reflectance of the MODIS reflective bands for 30 January 2004. R_k represents reflectance for band k .

30 January 2004			
MODIS Band (R_k)	Centre Wavelength (μm)	Mean R_k (dimensionless)	
		Cloud	Land
1 (R_1)	0.659	0.571	0.081
2 (R_2)	0.865	0.600	0.186
3 (R_3)	0.470	0.603	0.122
4 (R_4)	0.555	0.574	0.097
5 (R_5)	1.240	0.500	0.222
6 (R_6)	1.640	0.228	0.175
7 (R_7)	2.130	0.117	0.091
17 (R_{17})	0.905	0.095	0.139
18 (R_{18})	0.936	0.399	0.040
19 (R_{19})	0.940	0.357	0.072
26 (R_{26})	1.375	0.187	0.002



(a)



(b)

Fig. 1: Cloud spectral signature using reflectance data for 30 January 2004. (a) Plot of mean cloud reflectance without bands 8 – 17, and (b) Same as (a) but in term of wavelength to form the spectral signature of cloud and land, with MODIS band number in red font. Vertical bars indicate standard deviations.

To separate between cloud and non-cloud, a threshold value from the MODIS cloud mask was used and the cloud masking results for R_1 and R_{26} reflectance tests are shown in Fig. 2 (a) and (b). The raw data and masked data are shown in left and middle column, while the corresponding histogram, on the right column. For R_1 test, Fig. 2 (a(left)) clearly shows bright patches of opaque clouds in the east and south of Malaysia, while transparent clouds can be seen surrounding the opaque clouds. In Fig. 2 (a(right)), pixels with reflectance larger than the threshold were labelled as cloud and masked red. Pixels detected as cloud by R_1 test can be seen distributed throughout almost the whole Malaysia. These are low clouds, i.e. stratus, stratocumulus, cumulonimbus, cumulus and nimbostratus. The effectiveness of this test is due to the surface types, i.e. mainly vegetations, which possess much lower reflectance in $0.66 \mu\text{m}$ wavelength measurement; therefore separation between the cloud and cloud-free pixels can be done easily. For R_{26} test, Fig. 2 (b(left)) shows a much brighter but smaller cloud patches in the south and east of Malaysia and transparent clouds in between them. The Earth surface seems very dark due to the very low surface reflectance measured at $1.38 \mu\text{m}$ wavelength (i.e. near infrared), resulting in a high contrast between the clouds and their background. In Fig. 2 (b(right)), when mask is applied, more cloud pixels can be observed in the middle towards the north; clouds detected by this test are thin high clouds, i.e. cirrus, cirrostratus and cirrocumulus.

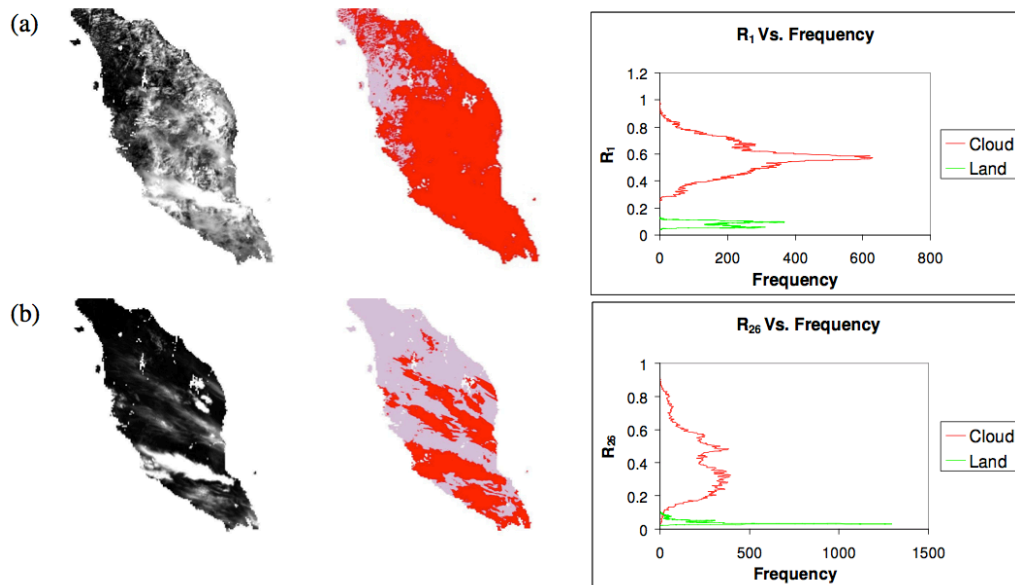


Fig. 2: (a) R₁ and (b) R₂₆ test for 30 January 2004 before (left) and after (middle) applying the thresholds with the cloud pixels masked in red, and the corresponding histogram for cloud and land (right). Cloud-free and water body pixels are masked grey and white respectively.

Cloud Detection Using Brightness Temperatures:

Conversion from radiance to brightness temperature was carried out for all 16 thermal bands using Eq. 1. The mean brightness temperatures values for each of the thermal MODIS bands are shown in Table 2 (MODIS Characterization Support Team, 2006).

$$L = \frac{2hc^2\lambda^{-5}}{\left(e^{\frac{hc}{k\lambda T}} - 1\right)} \quad (1)$$

where L = radiance ($\text{Wm}^{-2}\mu\text{m}^{-1}\text{sr}^{-1}$)
 h = Planck's constant (Js) = 6.626×10^{-34} Js
 c = speed of light in vacuum (ms^{-1}) = 3×10^8 ms^{-1}
 k = Boltzmann gas constant (JK^{-1}) = 1.381×10^{-23} JK^{-1}
 λ = band or detector centre wavelength (μm)
 T = brightness temperature (K)

Table 2: Cloud and land mean brightness temperature of the MODIS thermal bands for 30 January 2004. BT_k represents brightness temperature for band k .

MODIS Band (BT_k)	Wavelength (μm)	30 January 2004	
		Mean BT_k (K)	
		Cloud	Land
20 (BT_{20})	3.750	269.964	306.490
21 (BT_{21})	3.959	254.896	304.237
22 (BT_{22})	3.959	249.560	303.843
23 (BT_{23})	4.050	245.129	299.746
24 (BT_{24})	4.465	229.749	256.047
25 (BT_{25})	4.515	232.711	277.244
27 (BT_{27})	6.715	227.489	250.893
28 (BT_{28})	7.325	232.098	263.732
29 (BT_{29})	8.550	237.042	294.706
30 (BT_{30})	9.730	235.807	277.727
31 (BT_{31})	11.030	235.607	296.679
32 (BT_{32})	12.020	234.682	294.901
33 (BT_{33})	13.335	230.818	270.227
34 (BT_{34})	13.635	228.322	258.166
35 (BT_{35})	13.935	226.383	249.858
36 (BT_{36})	14.235	220.722	231.596

Curves of brightness temperature for the thermal MODIS bands for cloud and land against band number and wavelength are shown Fig. 3 (a) and (b) respectively. Each point in (b) corresponds to that of (a) consecutively. Land exhibits a brightness temperature ranging from approximately 231 to 306 K shows a sharp increase between 4 and 5 μm , then a fluctuating trend at longer wavelengths. The cloud brightness temperature is nearly constant in the lower-numbered bands but increases at longer wavelengths.

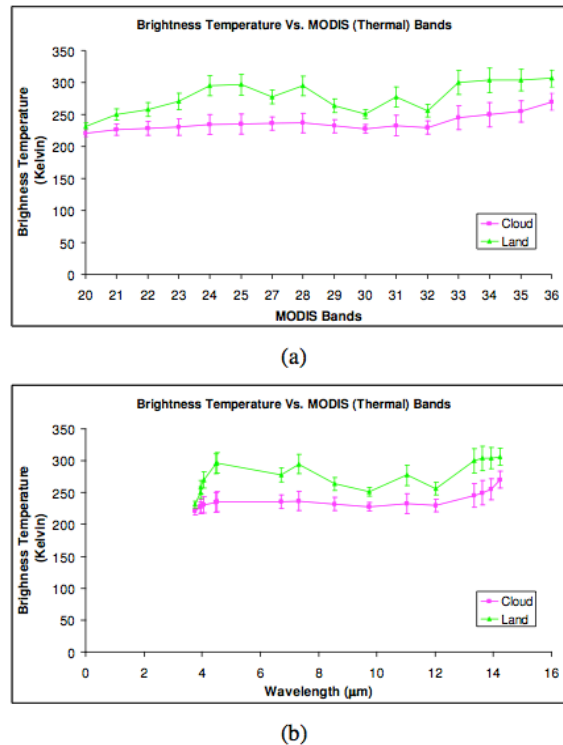


Fig. 3: Brightness temperature for cloud and land for MODIS Terra data dated 30 January 2004 plotted against (a) MODIS bands and (b) wavelength. Here, the points in (b) consecutively correspond to those in (a). Vertical bars indicate standard deviations.

Brightness temperature tests using BT27 and BT35 were applied to the MODIS dataset from 30 January 2004. Fig. 4 shows (a) BT27 and (b) BT35 tests for 30 January 2004 before (left) and after (right) applying the thresholds with the cloud pixels masked in red; cloud-free and water body pixels are masked grey and white respectively. Fig. 4 (a(left)) shows dark patches of cloud by BT27 in the south of Malaysia and much smaller patches can be seen in the east of Malaysia. In Fig. 4 (a(right)), the red masks are located about the same place where the black patches are found – almost no cloud is found elsewhere. Quite similar outcomes are shown by BT35 Fig. 4 (b) due to the quite similar spectral response to cloud; both tests are sensitive to thick high clouds, e.g. cumulonimbus.

Cloud Detection Using Brightness Temperature Difference:

Brightness temperature difference tests using BT31 - BT32 and BT31 - BT22 were applied to the MODIS dataset. For BT31 - BT32 test, cloud can hardly be seen by visual analysis of Fig. 5 (a(left)). In Fig. 5 (a(right)), when the mask was applied, most clouds are detected in the east of Malaysia. Clouds detected by this test were thin high clouds, e.g. cirrus, cirrostratus and cirrocumulus. In Fig. 5 (b(left)), for BT31 - BT22 test, it seems that only a few cloud patches are visible in the middle and south of Malaysia; pixels detected as cloud can be seen throughout the whole Malaysia when the mask was applied (Fig. 5 (b(right))). Clouds detected by BT31 - BT22 are thick low clouds, e.g. cumulonimbus and cumulus, which the former brings heavy downpour in Malaysia during the Northeast monsoon season.

It is useful to know the amount of cloud captured by each test so we can assess its effectiveness. Hence, for each test we calculate the amount of cloud in terms of area (km^2) and percentage land area (%). All cloud tests used and the amount of cloud captured on 30 January 2004 are given in Table 3. R1 gives the largest area, i.e. 84% of the land or $121,549 \text{ km}^2$. This is followed by the BT31 - BT22 with 82% ($119,968 \text{ km}^2$) and the BT29 - BT31 test with 70% ($102,370 \text{ km}^2$). The least clouds are detected by the BT27, 7% ($9,549 \text{ km}^2$) and BT35, 9% ($13,522 \text{ km}^2$). The 84% captured by the R1 test is due to the various types of cloud that are detectable in 0.66 μm wavelength; this owing to the much higher difference in cloud and vegetation spectral properties.

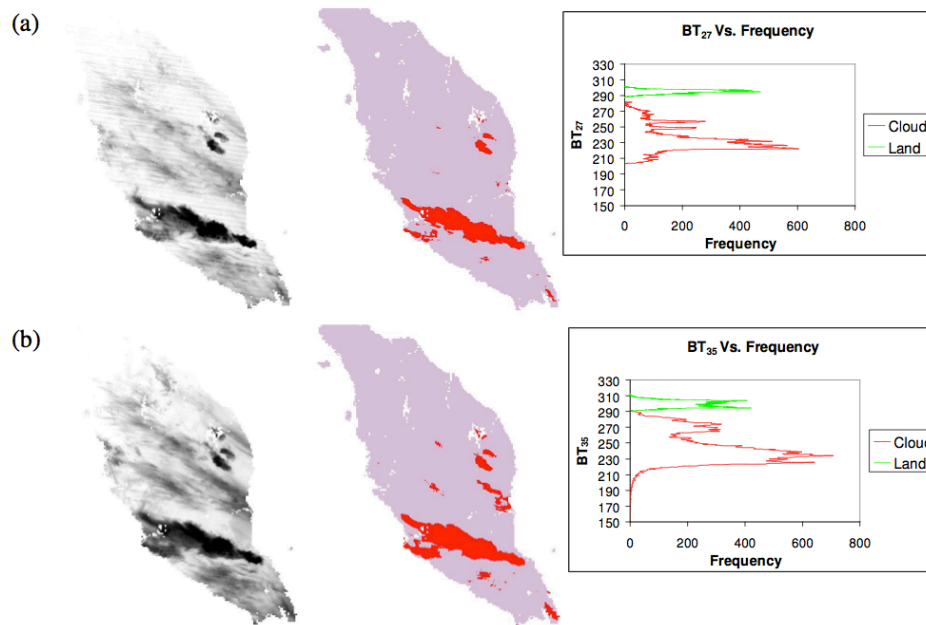


Fig. 4: (a) BT₂₇ and (b) BT₃₅ tests for 30 January 2004 before (left) and after (right) applying the thresholds with the cloud pixels masked in red. Cloud-free and water body pixels are masked grey and white respectively.

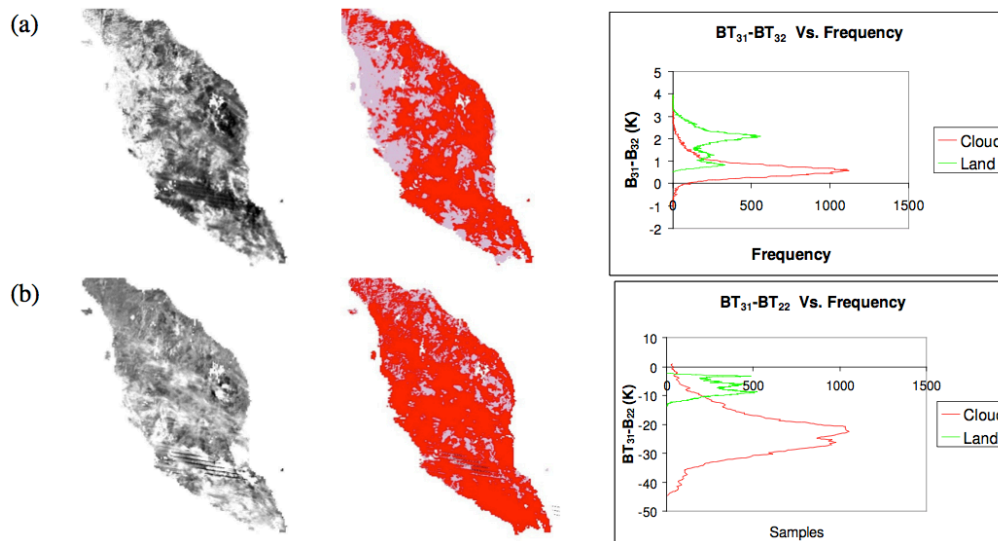


Fig. 5: (a) BT₃₁ - BT₃₂ and (b) BT₃₁ - BT₂₂ tests for 30 January 2004 before (left) and after (right) applying the thresholds with the cloud pixels masked in red. Cloud-free and water body pixels are masked grey and white respectively.

Table 3: Cloud tests and area covered for 30 January 2004.

Mask type	MODIS Test (based on band number)	Same as the second column, but based on wavelengths	Area	
			(km ²)	Percentage of cloud from land area (%)
Cloud mask	BT ₂₇	BT _(6,7)	9549	6.6
	BT ₃₅	BT _(13,9)	13522	9.3
	BT ₃₁ - BT ₃₂	BT ₍₁₁₎ - BT ₍₁₂₎	90627	62.3
	BT ₃₁ - BT ₂₂	BT ₍₁₁₎ - BT _(3,9)	119968	82.5
	R ₁	R _(0,66)	121549	83.6
	R ₂₆	R _(1,38)	52406	36.0

To further verify the result, we examine the mask in term of overlapping tests, we segmented the mask based on the number of tests that occurred (Fig. 6). It can be seen that the three-tests overlapping covers the

largest area (36%) followed by the two-tests overlapping (24%) and the four-tests overlapping (16%), while the five-tests overlapping has the smallest area (4%). The six-tests overlapping (5%) occurs at the middle southern parts of Malaysia (southern Pahang, northern Johor and southern Selangor) – this indicates that several types of cloud occurred simultaneously over these areas. This is consistent with the fact that these areas received much higher rain than other areas during January every year (Wong *et al.*, 2009).

Number of test	Percent cloud from land area	Area (km ²)	
No cloud	3.4	4943	Grey
1	12.5	18174	Blue
2	23.7	34458	Cyan
3	35.7	51905	Yellow
4	16.0	23263	Magenta
5	3.7	5380	Maroon
6	5.0	7270	Green

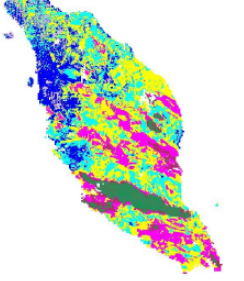


Fig. 6: The cloud mask for 30 January 2004 classified based on the number of overlapping tests; the colours (blue, cyan, yellow, magenta, maroon and green) are associated with the number of tests, while non-cloud and water pixels are masked grey and white respectively.

Conclusion:

A method for detection and masking localised cloud was developed by making use of measurements made from reflective, thermal and brightness temperature difference of thermal bands. Spectral analysis based on histogram thresholds was carried out and found able to detect clouds over the tropical regions effectively. The analysis of overlapping tests was found consistent with the fact that more types of cloud occurred in areas that received much higher rain than other areas.

ACKNOWLEDGMENTS

We would like to thank Universiti Teknikal Malaysia Melaka and Malaysian Ministry of Higher Education for funding this study under the FRGS Grant (Project No.: FRGS/2012/FTMK/TK06/03/02 F00143).

REFERENCES

- Ackerman, S.A., K.I. Strabala, W.P. Menzel, R.A., Frey, C.C. Moeller, L.E. Gumley, B.A. Baum, C. Schaaf and G. Riggs, 2002. Discriminating Clear-Sky from Cloud with MODIS - Algorithm Theoretical Basis Document. Products: MOD35. ATBD Ref. No.: ATBD-MOD-06: MODIS Cloud Mask Team.
- Ahmad, A. and S. Quegan, 2012. Analysis of maximum likelihood classification on multispectral data. *Applied Mathematical Sciences*, 6(129): 6425-6436.
- Ahmad, A. and S. Quegan, 2013. Comparative Analysis of supervised and unsupervised classification on multispectral data. *Applied Mathematical Sciences*, 7(74): 3681-3694.
- Ahmad, A. and S.F. Sufahani, 2012. Analysis of Landsat 5 TM data of Malaysian land covers using ISODATA clustering technique, *Proceedings of the 2012 IEEE Asia-Pacific Conference on Applied Electromagnetic (APACE 2012)*, pp: 92-97.
- Bendix, J., R. Rollenbeck and W.E. Palacios, 2004. Cloud detection in the Tropics – a suitable tool for climate – Ecological studies in the high mountains of Equador. *International Journal of Remote Sensing*, 25(21): 4521-4540.
- Choi, Y.-S. and C.-H. Ho, 2009. Validation of the cloud property retrievals from the MTSAT-1R imagery using MODIS observations. *International Journal of Remote Sensing*, 30: 5935-5958.
- Di Vittorio, A.V. and W.J. Emery, 2002. An automated, dynamic threshold cloud-masking Algorithm for daytime AVHRR images over land. *IEEE Transactions on Geoscience and Remote Sensing*, 40(8): 1682-1694.
- Hashim, M., K.D. Kanniah, A. Asmala and A.W. Rasib, 2004. The use of AVHRR data to determine the concentration of visible and invisible tropospheric pollutants originating from a 1997 forest fire in Southeast Asia. *International Journal of Remote Sensing*, 25(21): 4781-4794.
- Jose, A.T.A., G.R. Francisco, P.L. Mercedes and M. Canton, 2003. An automatic cloud-masking system using backpro neural nets for AVHRR scenes. *IEEE Transactions on Geoscience and Remote Sensing*, 41(4): 826-831.

Li, J., W.P. Menzel, Z. Yang, R.A. Frey and S.A. Ackerman, 2003. High-spatial-resolution surface and cloud-type classification from MODIS multispectral band measurements. *Journal of Applied Meteorology*, 42: 204-226.

Logar, A.M., D.E. Lloyd, E.M. Corwin, M.L. Penaloza, R.E. Feind, T.A. Berendes, K. Kuo and R.M. Welch, 1998. The ASTER polar cloud mask. *IEEE Transactions on Geoscience and Remote Sensing*, 36(4): 1302-1312.

MODIS Characterization Support Team, 2006. MODIS Level 1B Product User's Guide: For Level 1B Version 5.0.6 (Terra) and Version 5.0.7 (Aqua). MD, USA: NASA/Goddard Space Flight Center.

Rossow, W.B., A.W. Walker and L.C. Gardner, 1993. Comparison of ISCCP and other cloud amounts. *Journal of Climate*, 6: 2394-2418.

Saunders, R.W., 1986. An automated scheme for the removal of cloud contamination from AVHRR radiances over Western Europe. *International Journal of Remote Sensing*, 7: 867-886.

Wong, C.L., R. Venneker, S. Uhlenbrook, A.B.M. Jamil and Y. Zhou, 2009. Variability of rainfall in Peninsular Malaysia. *Hydrological and Earth System Science Discussion*, 6: 5471-5503.